Low Frequency Oscillation Analysis of a Hall Thruster Using a One-Dimensional Hybrid-Direct Kinetic Simulation

IEPC-2013-266

Presented at the 33^{rd} International Electric Propulsion Conference, The George Washington University, Washington, D.C., USA October 6–10, 2013

Kentaro Hara* and Iain D. Boyd †
University of Michigan, Ann Arbor, MI 48109-2140

A one-dimensional hybrid-direct kinetic (DK) simulation is used to analyze the low frequency oscillation mode of a Hall thruster. The advantage of the DK simulation, which solves the kinetic equations to obtain the velocity distribution function directly, is that numerical noise due to the use of computational particles in kinetic particle simulations is greatly reduced. Thus, a wide variety of frequency oscillation modes can be captured more accurately. Additionally, in order to reduce the numerical error of the kinetic solver, we have developed a front tracking method that captures the maximum velocity of particles to track the evolution of the VDFs on a fixed discretized phase space. The numerical results show that the low frequency discharge oscillation as a function of magnetic field strength agrees well with experiments in which a transition from a breathing mode to a stable mode is observed. Electronically excited atoms are modeled in a transient numerical simulation, which allows one to analyze the light intensity that is often measured in experiments. The possibility of anomalous diffusion coefficient as a parameter of plasma parameters at different Hall thruster operation is discussed.

I. Introduction

The partially magnetized plasma in Hall thrusters experiences complex processes such as plasma-wall interaction, anomalous diffusion due to strong magnetic fields, ionization and acceleration of ions, and a variety of collisions. These phenomena result in a wide range of various plasma oscillation modes as summarized by Choueiri.[1] In order to understand the nonlinear transport of a Hall thruster plasma, it is required to analyze and capture the high-frequency oscillations. In addition to obtaining high frequency data experimentally, a numerical simulation can be very useful in understanding the dynamic behavior of the discharge plasma in a Hall thruster.

Fluid and particle methods have been well developed in the electric propulsion community. Due to the non-equilibrium nature of a Hall thruster plasma, fluid models may not be able to capture some of the important effects caused by non-Maxwellian distribution of the plasma species. For instance, ionization and acceleration regions in Hall thrusters overlap so that the VDFs of ions are inherently non-Maxwellian. On the other hand, particle simulations are very useful to model non-equilibrium plasmas but suffer from the inherent statistical noise resulting from computational particles, often called macro-particles. Statistical noise results in numerical heating of the plasma for a fully kinetic method and cannot capture the VDFs smoothly due to the use of macro-particles. Even in hybrid methods, in which particle methods are used for ions and a fluid model is used for electrons, the statistical noise yields non-smooth macroscopic plasma properties. Time averaging techniques are often used in existing hybrid methods so that oscillatory behavior may not be resolved by particle methods.

*Graduate Student, Department of Aerospace Engineering. kenhara@umich.edu
†Professor, Department of Aerospace Engineering.

It has been recently shown that a direct kinetic (DK) simulation[2] that solves the kinetic equations directly is more useful in comparison to existing particle methods to capture low and high frequency oscillation modes. The VDFs are obtained directly on a discretized phase space so that the statistical noise due to discrete macro-particles is reduced. Collisionless direct kinetic simulations, often call Vlasov simulations, are also of great interest in other plasma applications ranging from weakly ionized plasma[3] to high temperature plasmas used in inertially confined plasma.[4] In this paper, low frequency oscillations are investigated using a one-dimensional (1D) hybrid-DK simulation in which a DK simulation is used for ions and a fluid model is used for electrons. Although radial and azimuthal plasma transport is not solved directly, plasma oscillations in the axial direction that affect the discharge oscillation are still not completely understood. In particular, it has been observed that a Hall thruster operates at different modes depending on the discharge voltage, mass flow rate, and magnetic field strength.[5–8] Sekerak *et al.* showed that there is a transition in oscillation modes from a strong axial ionization mode, which is often called a breathing mode, at small magnetic fields, to a more stable operation at intermediate magnetic fields.[7]

The main purpose of this paper is to analyze the mode transition of an SPT-100 thruster using a hybrid-DK simulation. The present hybrid-DK simulation is improved from the previous model developed by Hara *et al.*[2] Section II focuses on the discharge plasma model used in the simulation. In Section III, the numerical scheme of the DK simulation and the newly developed front tracking method are described. Finally, in Section IV, results obtained from the hybrid-DK simulation are presented and discussed.

II. Hybrid-DK Simulation

The discharge plasma of a SPT-100 Hall thruster is modeled using a 1D hybrid-DK simulation. A DK simulation is used for ions, a fluid model which solves the momentum and energy equations is used for electrons, and neutral atoms are modeled solving the continuity equation.

The radial and azimuthal transport is not directly modeled in this paper. As the magnetic field of the SPT-100 shows in Figure 1,[9] the magnetic field lines are relatively straight inside the channel and in the near plume. Thus, a 1D simulation represents some of the important physical phenomena in the axial direction.

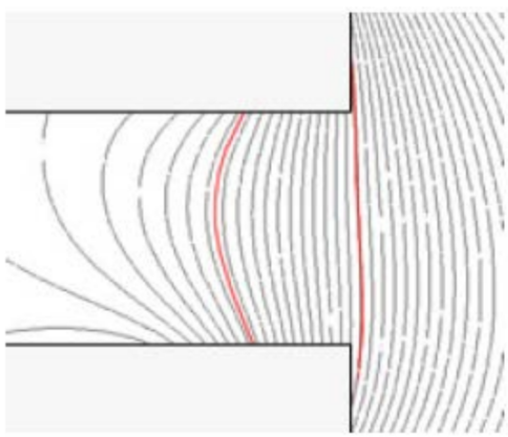

Figure 1. The magnetic field of SPT-100. Reproduced from Ref. 9

A. Ion kinetic equation

The Lorentz force can be neglected for ions in the channel of a Hall thruster since the magnetic field strength is chosen so that ions are non-magnetized relative to the electrons.

The present one-dimensional (1D) DK simulation includes one dimension in both space and velocity (1D1V). The ion transport equation is given by

$$\frac{\partial f_i}{\partial t} + v_x \frac{\partial f_i}{\partial x} + \frac{eE_\perp}{m_i} \frac{\partial f_i}{\partial v_x} = S \tag{1}$$

where $E_\perp$ is the axial electric field, e is the elementary charge, m_i is the mass of a xenon ion, f_i is the VDF of ions, and S is the collision term. The collision term, S, includes the ionization from ground state atoms and metastables, which is described in the next section. Multiply charged ions are not included in the model. In order to calculate the collision rates and to employ the electron fluid models, the macroscopic quantities, such as number density and mean velocity, are obtained by evaluating moments of the ion VDFs:

$$n_i(x,t) = \int f_i(x, v_x, t) dv_x \tag{2}$$

$$u_i(x,t) = \int v_x \hat{f}_i(x, v_x, t) dv_x \tag{3}$$

where n_i and u_i are the number density and mean velocity of ions, respectively, $\hat{f}$ is the normalized VDF. The numerical method for solving Eq. 1 is described in Sec. III

B. Neutral atom equation

The low frequency oscillation of a Hall thruster plasma is affected mainly by the interaction of ion and electron transport but also by the transport of neutral atoms. It has been recently shown in a 1D hybrid-DK simulation[2] that the neutral atom modeling also affects the breathing mode frequency and magnitude. For instance, the breathing mode frequency increases when a DK method is used instead of a fluid model for neutral atoms because of the accelerated neutral atoms in the ionization and acceleration regions due to selective ionization.

In addition, the use of a ultra-fast cameras allows one to experimentally observe the evolution of the light emitted from the Hall thruster plasma.[7,10,11] Light is emitted due to the de-excitation of electronically excited states to a lower energy level. A numerical model that accounts for an excited state can be used to directly compare the light intensity obtained by experiments with the numerical results.

The continuity equation is solved for the ground state and metastable xenon atoms.

$$\frac{\partial n_s}{\partial t} + v_n \frac{\partial n_s}{\partial x} = \sum_j n_s n_j k_j \tag{4}$$

where k_j is the rate coefficient of the collision which is a function of electron mean energy. Eq. 4 is solved using a first-order upwind method with a constant velocity, $v_{n0} = 250$ m/s.

The metastable xenon atoms, or the electronically excited atoms, and the reactions of xenon are fully described in Ref. 12. Here, in the present simulation, one type of metastable atom species is assumed for simplicity. The reactions are shown in Table 1. Only singly charge ions are taken into account and the multiply charged ions are neglected.

Table 1. Collisions: Xe, Xe^*, and Xe^+ are the ground-state atom, metastable, and ion.

				Rate coefficient	Energy lost	Cross section
Excitation	$Xe + e$	$\rightarrow$	$Xe^* + e$	Fig. 2	8.3 eV	Ref. 13.
Direct ionization	$Xe + e$	$\rightarrow$	$Xe^+ + e$	Fig. 2	12.1 eV	Ref. 14.
Stepwise ionization	$Xe^* + e$	$\rightarrow$	$Xe^* + e$	Fig. 2	3.8 eV	Ref. 15.
Deexcitation	Xe^*	$\rightarrow$	$Xe + h\nu$	1×10^7 s^{-1}	-	Ref. 12.

Stepwise ionization from the metastable atom is assumed to follow the rate coefficient of $Xe(^3P_2) + e \rightarrow Xe^+ + e + e$, which is given in Ref. 15. The spontaneous emission reactions that emit photons in Ref. 12 are (1) de-excitation from highly excited states (the sum of the $6s^1$, $6p$, $5d$, $7s$ states) to the first two excited states, $Xe^*(^3P_2)$ and $Xe^*(^3P_1)$, and (2) de-excitation from the resonant state $Xe^*(^3P_1)$ to the ground state, Xe. Rate coefficients for the two spontaneous emission are 3×10^7 s^{-1} and 2.7×10^6 s^{-1}, respectively. As one metastable in this simulation is accounted for, the de-excitation rate of the metastable is assumed to 1×10^7 s^{-1}. Inclusion of other electronically excited states will be left for future work.

Figure 2 shows the collision rates of the direct ionization, excitation, and stepwise ionization, as a function of electron mean energy. In the simulation, the rate coefficients are pre-calculated assuming a Maxwellian distribution for electrons and using the cross section data shown in Table 1.

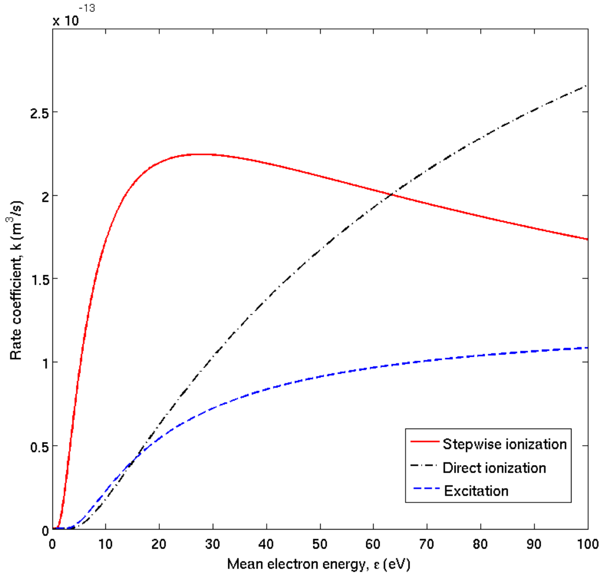

Figure 2. Collision rates of xenon atoms

C. Electron momentum equation

A quasi-neutral assumption is employed for the electron momentum and energy equations. The characteristic time scale for electron transport is assumed to be much smaller than that of ions so that a steady state assumption is also used for electrons.

The 1D electron momentum equation is described by

$$v_{ex} = \mu_{eff}\left[E_x - \frac{1}{n_e}\frac{\partial}{\partial x}(n_e T_e)\right] \tag{5}$$

where μ_{eff} is the effective electron mobility and v_{ex} is the axial electron mean velocity, which is obtained from the current conservation:

$$I_d = enA(v_{ix} - v_{ex}) \tag{6}$$

where I_d is the discharge current, n is the plasma density which is equal to the ion density, and A is the cross sectional area of the channel. The discharge current is obtained from integrating Eq. 5 using Eq. 6, which is described in Ref. 2 in detail.

Based on the previous model, the pressure term is included in order that ions drift toward the anode as Ahedo *et al.* pointed out.[16] Without the pressure term, there is no mechanism that drives the ions back to the anode in order to form an anode sheath although the sheath is not resolved in the present model. The electron drift is usually much smaller than the electron thermal velocity so that the contribution inertia term can be assumed to be negligible.

1. Electron mobility

In solving Eq. 5, the electron mobility mostly affects the properties of the Hall thruster plasma. In this study, due to the magnetic field of the SPT-100 shown in Fig. 1, the effective electron mobility can be written as a sum of the parallel and perpendicular electron mobilities:

$$\mu_{eff} = \xi(x)\mu_\perp + (1 - \xi(x))\mu_\parallel \tag{7}$$

where $\mu_\perp$ and $\mu_\parallel$ are the electron mobility across and along the magnetic field, respectively. $\xi(x)$ is the geometerical factor that is chosen to account for the actual shape of the magnetic field. The magnetic field is radially aligned from the middle of the channel to the near-plume. However, it can be seen that the magnetic field near the anode is curved and the magnetic field line intersects with the anode almost perpendicularly.

As electrons move along magnetic field lines and cross-field motion is suppressed, the near-anode region should be modeled using the parallel electron mobility. Without the contribution from the parallel electron mobility, the plasma cannot be effectively confined inside the channel due to the low mobility near the anode. In the simulation, it is set between $\xi(0) = 0$ and $\xi(0.4 \times L) = 1$ where L is the channel length. $x = 0.4 \times L$ is chosen arbitrary.

The parallel and perpendicular electron mobilities are written as

$$\mu_{\perp} = \frac{e}{m_e \nu_{eff}} \frac{1}{1 + (\omega_b/\nu_{eff})^2} \tag{8}$$

$$\mu_{\parallel} = \frac{e}{m_e \nu_{eff}} \tag{9}$$

where the effective collision frequency is

$$\nu_{eff} = \nu_{e-n} + \nu_{ew} + \nu_{ano} + \nu_{e-i}$$

where ν_{e-n}, ν_{ew}, ν_{ano}, ν_{e-i} are the collision frequencies of electron-neutral momentum transfer, electron-wall collisions, anomalous diffusion, and Coulomb collisions, respectively.

2. *Electron-neutral collisions*

The electron-neutral momentum transfer includes elastic and inelastic collisions.

$$\nu_{e-n} = (\beta_{el}(\epsilon) + \beta_{inel}(\epsilon)) n_n$$

where $\beta(\epsilon)$ is the rate coefficient calculated assuming a Maxwellian distribution for electrons and subscripts *el* and *inel* represent elastic and inelastic collisions respectively. β_{el} and β_{inel} are a function of the electron mean energy, ϵ, which are given in Fig. 2. The rate coefficient of momentum transfer collisions is obtained by using the cross section data of Hayashi.[17]

3. *Electron-wall collisions*

Barral *et al.* suggested an electron-wall collision model based on the fluid sheath theory.[6,18] For a steady state sheath, Bohm's condition should be satisfied at the sheath edge. Thus, it is required that the ion velocity at the sheath edge has a velocity larger than the ion acoustic speed towards the wall. As the incident electron current increases due to the secondary electrons from the wall, the current of the incident electrons that collide with the wall also increases. The collision frequency is given by

$$\nu_{ew} = \frac{1}{R_o - R_i} \sqrt{\frac{T_e}{m_i}} \frac{1}{1 - \sigma} \tag{10}$$

where R_o is the outer radius and R_i is the inner radius of the Hall thruster channel, and σ is the effective secondary electron emission (SEE) rate, which is a function of the electron temperature. The SEE model is identical to[6,18] in which the wall material is BN-SiO_2 and the effective SEE rate is $\sigma = \max(2T_e/50, 0.986)$ where T_e is the electron temperature.

4. *Anomalous collisions*

It has been suggested by many authors in the Hall thruster community that the electron mobility should be larger than the classical theory from an experimental observation, i.e., the electric field is larger inside the channel than in the plume outside the channel.[19–22] Although there is not yet any self-consistent model that describes the anomalous conductivity, the authors usually reference experiments and theories developed in the 1960s. One example is the experiment by Yoshikawa and Rose[23] in which the electron mobility across a magnetic field in an arc was shown to lie between the classical theory ($\mu \sim B^{-2}$) and the Bohm diffusion ($\mu \sim B^{-1}$) in the range of 250 G $\leq$ B $\leq$ 1000 G.

Here in the present model, we choose anomalous mobility models for outside and inside the channel.

$$\nu_{ano,outside} = \frac{1}{16}\omega_B$$

$$\nu_{ano,inside} = \frac{1}{160}\omega_B$$

This model is a two-region model which is also employed by Hagelaar *et al.*[22] and Koo and Boyd.[21] It has been recently shown that a three-region model for the electron mobility shows good agreement with the plasma properties obtained in the H6 thruster.[19] Although it is possible to find the anomalous mobility coefficients that agree with experimental data, a self-consistent model that accounts for the anomalous diffusion without using empirical coefficients is required to understand the complex Hall thruster plasma. The main purpose of this paper is not to show agreement of the thruster performance but to capture the mode transition from a breathing mode to a stable mode that has been observed experimentally when the magnetic field is varied. The effect of the anomalous diffusion coefficient is discussed in Section IV-F in detail.

5. *Coulomb collisions*

Coulomb collisions are also included in the model. Electron-electron collisions occur twice as frequently as electron-ion collisions but their contribution to electron momentum transfer is small due to the small mass. Thus, the electron-electron collisions are neglected. Since small angle scattering is dominant for electron-ion Coulomb collisions, the Coulomb collisions that affect electron momentum transfer involve only large angle scattering. For a scattering angle $\theta \sim 90^\circ$, the collision frequency is given in SI units by

$$\nu_{ei} = n_i \frac{2.9 \times 10^{-12}}{T_{e,eV}^{1.5}} \ln \Lambda \tag{11}$$

where $T_{e,eV}$ is the electron temperature in electron-volt and $\ln \Lambda$ is the Coulomb logarithm. Coulomb collisions are only important at small electron temperature and large plasma density.[24]

D. Electron energy equation

It is assumed that electron energy is also steady in the time scale of ion transport. The simplified 1D electron energy equation reduces to an ordinary differential equation:

$$\frac{\partial}{\partial x}\left(\frac{5}{3} n v_{ex} \epsilon\right) = n_e v_{ex} E_\perp - n_e \left[\nu_{ew}\epsilon_w + \sum_j \nu_j \Delta\epsilon_j\right] \tag{12}$$

where ϵ is the mean electron energy, ν_{ew} is the electron-wall collision frequency given in Eq. 10, ϵ_w is the energy loss to the wall, ν_j is the collision frequency and $\Delta\epsilon_j$ is the energy loss due to an inelastic collision, j. The energy loss to the wall is given by

$$\epsilon_w = 2T_e + e|\phi_w|$$

where T_e is the electron temperature and ϕ_w is the sheath potential, which is a function of electron temperature and the SEE rate.[18,24]

The mean electron energy can be decomposed into

$$\epsilon = \frac{3}{2}T_e + \frac{1}{2}m_e(v_{ex}^2 + v_{e\theta}^2) \tag{13}$$

where $v_{e\theta}$ is the azimuthal velocity calculated as a product of the axial electron velocity v_{ex} and the Hall parameter $\Omega = \omega_B/\nu_{eff}$. Barral *et al.* solved the electron azimuthal transport equation additionally but it has been observed that the numerical solution and the assumption of $v_{e\theta} = v_{ex}\Omega$ show a good agreement.[18] In addition, it is assumed that the electron temperature is isotropic, i.e. $T_{e,\perp} = T_{e,\parallel}$ where $T_{e,\perp}$ and $T_{e,\parallel}$ are electron temperatures across and along the magnetic field, respectively.

The energy sink due to inelastic collisions is calculated by the collision rate, which is the product of number densities of the reacting species and rate coefficients shown in Fig. 2, and the threshold energy, $\Delta\epsilon$, for direct ionization, excitation, and stepwise ionization, shown in Table 1. The contribution of elastic collisions to the energy transport is very small due to the difference in ion and electron mass. Thus, the elastic collision term is neglected. In addition, for simplicity, thermal conductivity is also neglected in the present model. This assumption is based on the numerical results by Bareilles *et al.*[20] in which the contribution of heat conductivity is shown to be much smaller than the other terms remaining in Eq. 12. However, inclusion of the missing terms will be considered in future work.

III. DK simulation

A direct kinetic (DK) simulation solves Eq. 1 that is a multi-dimensional hyperbolic partial differential equation with a source term. The left and right hand sides are decoupled, similar to other numerical methods such as particle methods. The left hand side describes the particle transport in physical space and velocity space whereas the right hand side describes collisions.

A. Base scheme

The transport of the VDFs is solved on a discretized phase space, i.e. 1D in physical space (x) and 1D in velocity space (v). Strang- time splitting, which was first proposed by Cheng and Knoll,[25] is used. This gives second order accuracy in time integration. The left hand side of Eq. 1 reduces to a set of two 1D linear hyperbolic equations:

$$\partial_t f + v \cdot \partial_x f = 0,$$

$$\partial_t f + a \cdot \partial_v f = 0,$$

where a is the acceleration that is described by the electric field given in Eq. 5. In order to solve the linear advection equations, a finite volume method using flux reconstruction is employed. A modified Arora-Roe limiter that is based on a third-order accurate scheme to the linear advection equation (see Ref. 26) is used for the flux reconstruction. It has been shown that the Arora-Roe limiter is superior to other second-order total variation diminishing (TVD) limiters which preserve the positivity of the solution, $f(x, v, t) \geq 0$ for any x, v, and t.

B. Front tracking scheme

In addition to the previous work,[2] a front tracking method is employed in this paper. Usually for a DK or Vlasov simulation, maximum and minimum velocities of the calculation domain are set sufficiently large that the VDFs near those boundaries are close to zero. However, the numerical error, although it can be very small, can propagate in the calculation domain. The front tracking method keeps track of the maximum velocity allowed in each physical location. We refer to the interface between a very small number of VDF, ϵ_f, and 0 as a "front".

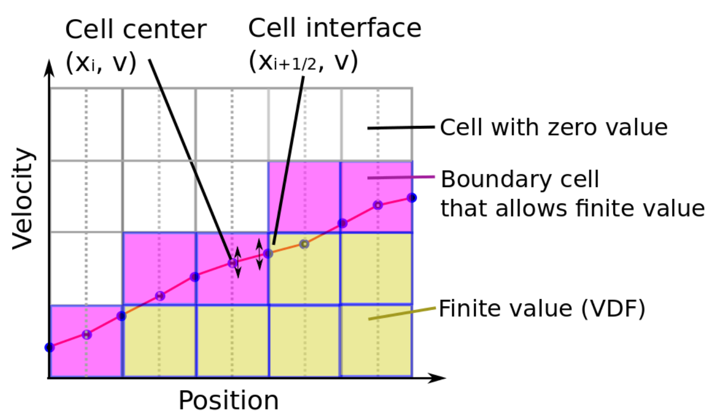

Figure 3. Illustration of the front tracking method

Target particles that can move in the velocity space are located at the cell interface and cell center of the physical space, as shown in Fig. 3. The front of the VDF is tracked by acceleration and deceleration of the target particles in velocity space and by the advection in physical space due to their own velocity. The velocity advection is done by simply adding and subtracting the velocity shift in each time step. Since the test particles are fixed on the cell center and interface, advection in physical space is not achieved by moving these particles in the physical space but by reconstructing a polynominal based on the location of test particles. Here, a third-order upwind method is used to update the particle information for the advection in physical space.

C. Ion VDFs

Figure 4 shows the comparison of instantaneous ion VDFs at the channel exit using a simplified electron fluid model used in Refs.[27] and.[2] Note that the electron fluid model used in this section is different from that in the following section. The results are shown in order to demonstrate the capability of the front tracking scheme.

The anode is set at $x = 0$, the channel exit is $x = 4$ cm, ions are generated with a velocity of 250 m/s for the hybrid-PIC simulation, a half-Maxwellian is used for the original hybrid-DK simulation, and a full-Maxwellian with a velocity shift of 250 m/s is used in the hybrid-DK simulation with the front tracking scheme. The negative ion velocities near the anode result from the use of full-Maxwellian in Fig .4(c). Instantaneous ion VDFs are evaluated at times where the discharge current is at its maximum. Although the discharge oscillation is not the same due to the difference in ion transport, it can be seen that the ions are ionized near the middle of the channel and accelerated toward the channel exit. The white zones represent

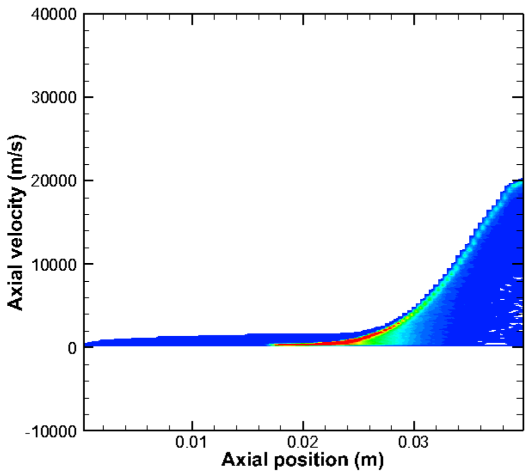

(a) Hybrid-PIC

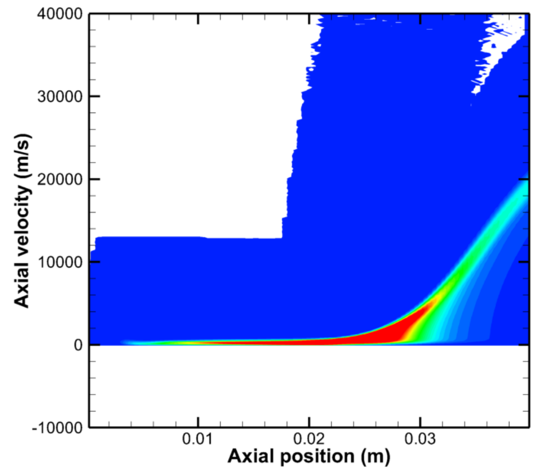

(b) Hybrid-DK (regular)

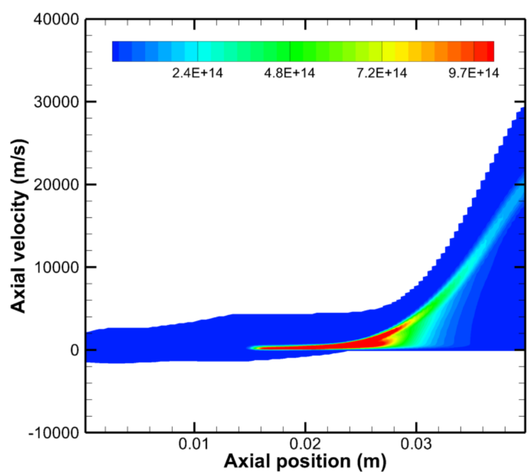

(c) Hybrid-DK (front tracking)

Figure 4. 1D1V ion VDF contours. The white zones represent VDFs below a very small number $f_i \sim 10^{-30}$ and the color scale is the same.

regions of phase space that have no particles, $f(x, v) = 0$.

The hybrid-PIC simulation[27,28] employed 300,000 particles in the calculation domain, which is 3,000 particles per cell on average. In spite of the large number of macro-particles, there are some empty cells near the channel exit, as shown in Fig. 4(a). The discretization of the hybrid-DK simulations is $\Delta x = 0.4$ mm, $\Delta v = 180$ m/s, and $\Delta t = 1$ ns. This corresponds to 100 cells and 400 cells in the physical and velocity space, respectively. The same spatial and temporal discretization are used in the hybrid-PIC simulation. Figure 4(b) shows the instantaneous ion VDFs obtained from a regular hybrid-DK simulation without front tracking. Significant dissipation in the large velocity region can be seen due to the numerical error. The small numerical error introduced propagates in the calculation domain and remains there. Finally, the results obtained from a hybrid-DK simulation with the front tracking method show that the maximum ion velocity is confined to a more physical range, as shown in Fig. 4(c). It can be seen that the maximum peak of the ion VDFs at the channel exit originates from the ionized plasma in the middle of the channel and there is also a small amount of ions that travel from the anode region in comparison to the hybrid-PIC result shown in Fig. 4(a). Using a front tracking method, the numerical results are greatly improved.

In addition, the computational time is also reduced by using a front tracking scheme. The computational wall time to run a physical time of 1 ms (100,000 timesteps) for each simulations is 3.6 hours, 1.6 hours, and 1.4 hours, for the hybrid-PIC, the hybrid-DK without a front tracking method, and the hybrid-DK with a front tracking method, respectively. In spite of the ratio of the number of particles and that of velocity bins being 3,000/400 = 7.5, the calculation time differs only by 3.6/1.6 = 2.25. The calculation time is not a one-to-one comparison between PIC and DK simulations since two additional steps are required to update the VDFs in a DK simulation. One step is to calculate the TVD limiter depending on the two adjacent cells and the other is to store the numerical flux at the cell interfaces. The calculation time of the hybrid-DK simulation with and without a front tracking method is nearly equal. The VDF outside the front is not calculated but at the same time the front must also be calculated in the front tracking method. Although the computational time is comparable in the two DK methods, the front tracking scheme can be faster because there is no extra computation for the small values introduced by numerical errors, which also are unphysical.

IV. Results

The axial transport of the plasma of a SPT-100 is modeled using a 1D hybrid-DK simulation with the front tracking method. The numerical setup and calculation domain are different from Sec. III-C.

The channel length is 2.5 cm, the outer radius is 5 cm, and the inner radius is 3.5 cm. This configuration is identical to the SPT-100ML thrusters. The calculation domain is chosen from $x = 0$ cm, the anode, to $x = 3.5$ cm, which is 1 cm away from the channel exit. It is also assumed that $x = 3.5$ cm is the cathode line where the electron mean energy is 6 eV and the potential is 0 V. The magnetic field is peaked at the channel exit and has a Gaussian shape identical to Barral's 1D model.[18] The discharge voltage is 300 V, anode mass flow rate is 5.0 mg/s, and the peak magnetic field is varied from 110 G to 200 G. Background pressure is not accounted for in this model.

The numerical parameters are $\Delta t = 1$ ns, $\Delta x = 2.5$ mm, and $\Delta v = 160$ m/s, which correspond to 1×10^6 time steps to reach 1 ms, with 140 cells in physical space, and 500 cells in velocity space. The simulation runs on a single processor computer and the calculation time is about 2.5 hours. This is consistent with the preliminary case in Sec. III-C where the total number of velocity bins is 40,000 whereas 70,000 bins are used in this section.

A. Dependency of magnetic field

Figure 5 shows the discharge mean current and the standard deviation of the oscillation. The anomalous mobility coefficients are fixed in all cases of the hybrid-DK simulation. The numerical results in Fig. 5(a) show a good agreement with the experimental data in Fig. 5(b) from B = 110 G to 200 G. The small magnetic field (B $\leq$ 110 G) and the large magnetic field (B $\geq$ 200 G) are not in agreement with the experiment. The discrepancy in the two regions is discussed.

As shown in Fig. 5(a), the optimal regime can be seen from $B \sim 135$ G to $B \sim 200$ G where the standard deviation of the discharge current oscillation is small. Below the optimal magnetic field ($B \sim 135$G), the mean discharge current and discharge oscillation magnitude increase as the magnetic field becomes weaker.

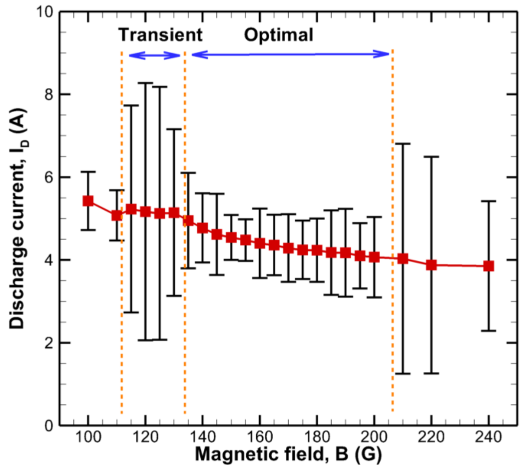

(a) Numerical results

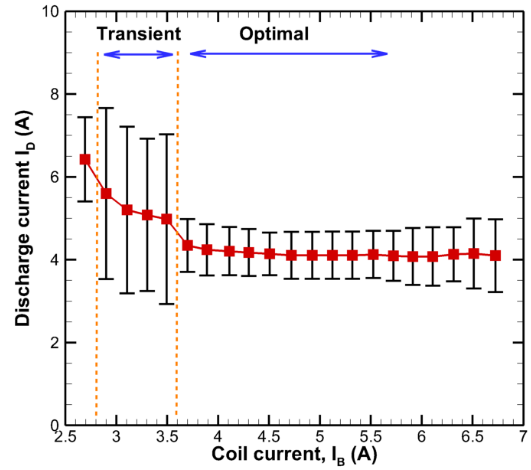

(b) Experiment: Reproduced from Ref. 29

Figure 5. Discharge current vs. magnetic field: Red symbol plots are the mean discharge current and error bars show the standard deviation.

There is a sharp increase in the discharge oscillation, which is indicated by the standard deviation of the discharge current.

As discussed in Sec. IV-B, the plasma oscillation is clearly different in the two regimes below and above B $\sim$ 135 G where mode transition occurs. This mode transition is consistent with experimental observations of the SPT-100 thruster[29, 30] and the H6 thruster.[7] Recently, Sekerak *et al.* showed that the mode transition strongly correlates with the global plasma transport in which azimuthally rotating spokes are dominant in a stable mode and moderate ionization oscillation is observed in a breathing mode. Although it is not possible to fully describe the multi-dimensional phenomena due to the 1D assumption in the present investigation, the observation of low frequency oscillations and the mode transition indicate some important physics and the missing factors to understand the plasma oscillation in a Hall thruster.

The oscillation modes for a constant discharge voltage have been first categorized by Tilinin.[31]

(I) Electron drift wave regime: When the magnetic field is small, the confinement of electrons follows classical conductivity, which is lower than anomalous conductivity, so that the discharge current is dominated by the electron current.

(II) Transition regime: The high frequency mode such as transit-time oscillations ($\sim$100kHz) causes high turbulent conductivity that results in enhanced electron mobility due to anomalous diffusion.

(III) Optimal regime: The thruster efficiency is maximized and stable operation is observed.

(IV) Regime of macroscopic instability: A jump in discharge current is observed for a larger magnetic field above the optimal magnetic field. It is also shown that the discharge current oscillation is very strong and it can even be recognized by the naked eye. The transition to the macroscopic instability is not as sharp in the H6[7] and in the SPT-100[30] is not as sharp as the observation of Tilinin.[31] It is claimed by Bechu *et al.* that the absence of this regime is an indicator of a robust design of the thruster.[30]

(V) Magnetic-saturation regime: the discharge oscillation is stable but noisy and chaotic. Due to the strong magnetic field, the gyroradius is much smaller and high frequency oscillation and turbulence become dominant.

As shown in Fig. 5(a), the transition regime (II), optimal regime (III), and macroscopic instability regime (IV) are observed in the numerical results. However, the other two regimes are not found when a fixed anomalous mobility model is used. The results suggest different mechanisms may be present in the other two regimes. The first regime (I) occurs when the electron conductivity is classical not anomalous.

Thus, a strong anomalous mobility may result in damping of the oscillations due to the larger mobility that results in smaller electric field as can be seen from Eq. 5. It is indicated by experiments that the last regime (V) occurs due to the chaotic motion that enhances anomalous mobility. A self-consistent mobility model in which the plasma properties determine the electron mobility is needed to understand the transition from a stable mode to a chaotic mode. The possible transition of the anomalous mobility coefficient is discussed in Sec. IV-F.

B. Breathing, stable, and strong ionization modes

In this section, the breathing mode observed in low magnetic field (B = 120 G) operation and the stable mode near the optimal magnetic field (B = 180 G) are compared. The electron components are reported as well as the heavy species components. Since the ion-DK solver reduces the statistical noise in particle methods, the integrated quantities such as ion density and mean velocity are obtained without the numerical noise.

The cause of the mode transition is under debate. It was suggested by Barral *et al.* that the mode transition due to magnetic field is attributed to a space charge limited sheath.[6] This mechanism was supported by experimental observations in which a different mode transition was observed for different wall materials.[5] However, Sekerak *et al.* recently showed that the mode transition is directly related to a transition from azimuthal rotating spoke dominant mode (low current, quiet) to axial breathing mode dominant mode (high current, oscillatory).

The numerical results also sugguest that mode transition may be correlated to a space charge limited sheath. However, since a space charge limited sheath is also observed in a strong ionization mode, the existence of a space charge limited sheath may not be the direct cause for the stabilization of the discharge oscillations.

1. Breathing mode

The results of a breathing mode (B = 120 G) are shown in Figure 6. This phenomenon has been widely observed experimentally and numerically.

It is obvious that in the breathing mode the ground-state atom density strongly fluctuates as shown in Fig. 6(a). Note that the oscillation cycle is not sinusoidal. Neutral atoms are resupplied more slowly than the burst of ionization. The speed of the resupply is characterized by the neutral flow speed. As the ionization proceeds, neutral atoms are lost quickly and the generation of ions and metastables is fast. The fast ionization is also correlated to the increase in electron mean energy, as shown in Fig. 6(e). As can be seen from Eq. 12, an increase in electron mean energy occurs due to the contribution of the energy loss being reduced by increased electron axial velocity (see Fig. 6(d)).

The metastable and ion densities oscillate as shown in Figs. 6(b) and 6(c), respectively. The magnitude of the two densities is different by an order of magnitude. The oscillation of these two quantities is in-phase and strongly correlated. It can be seen that the plasma is not perfectly confined in the ionization region and diffuses toward the anode. As shown in Fig. 6(d), the large electron axial velocity near the anode indicates that a large current of electrons is lost to the anode to balance the large ion current that is accelerated out toward the channel exit. In addition, the peak of the electron mean energy is about 45 eV that is equivalent to an effective electron temperature of 30 eV, which agrees with experimental observations: $T_e \sim 0.1V_d$.[32]

The location of the maximum peak of ion density is near $x = 0.01$ m where the electron mobility is almost discontinuous due to Eq. 7. As previously discussed, the electron mobility model can be improved to match the experimental results. For instance, Gascon *et al.* reported that the maximum ion density occurs at 4 -5 mm inside of the channel exit.[29] In the present investigation, it is chosen that the contribution of parallel conductivity starts from $x = 0.4L$ but realistically the magnetic field is still curved inside the channel, as shown in Fig. 1. The electron mobility model can be improved to match the experimental observations.

2. Stable mode

The plasma properties are stable in time in a stable mode (B = 180 G) as shown in Figure 7. The ground-state atoms do not exhibit a strong ionization oscillation as shown in Fig. 7(a). Metastable and ion densities are much reduced near the anode, as shown in Figs. 7(b) and 7(c), in comparison to the breathing mode. There is less diffusion of the plasma to the anode and the plasma is confined. The trend of metastable and

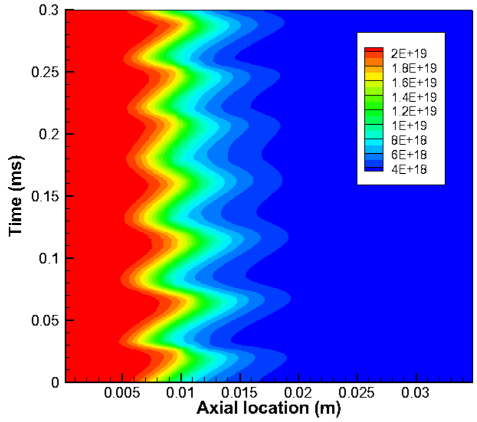

(a) Ground-state atom density (unit: m^{-3})

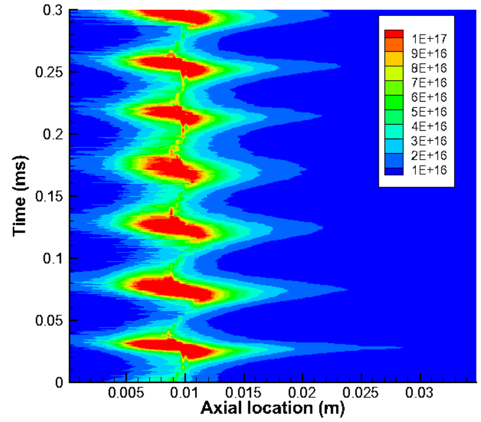

(b) Metastable density (unit: m^{-3})

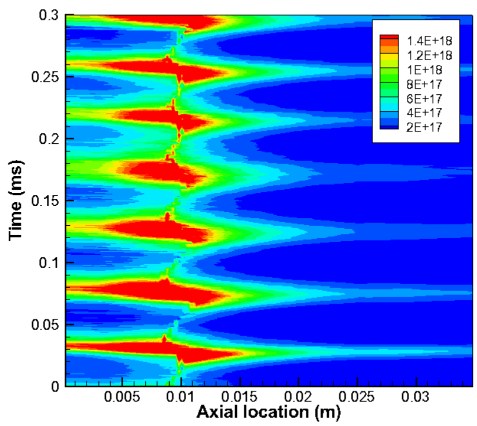

(c) Ion density (unit: m^{-3})

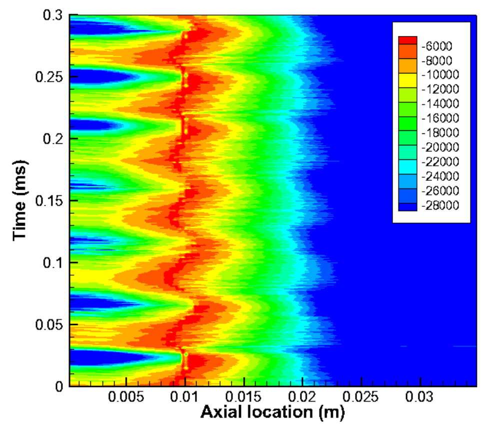

(d) Electron axial velocity (unit: m/s)

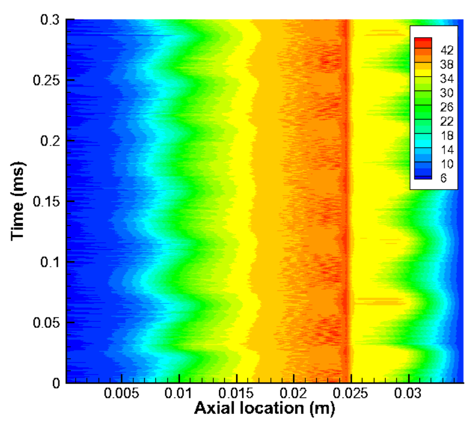

(e) Electron mean energy (unit: eV)

Figure 6. Breathing mode: B = 120 G

ion densities is in good agreement which indicates that the light intensity is proportional to and is in-phase with the ion density.

In comparison to a breathing mode, a reduced electron current in the axial direction in the near-plume can be observed from Fig. 7(d). The electron axial velocity in a stable mode is approximately 2.5 times smaller than that in a breathing mode. If the momentum transfer collisional frequency is assumed to be constant, the Hall parameter is 1.5 times larger for B = 180 G than for B = 120 G. This results in a decrease in the electron azimuthal velocity. As shown in Figs. 6(e) and 7(e), the peak of electron mean energy is almost the same. Thus, from Eq. 13, it can be seen that the electron temperature can be larger when the electron azimuthal component is small. As a result, in a stable mode, the electron temperature near the channel exit approaches the electron temperature that forms a space charge limited sheath. As can be seen from Eq. 10, a strong SEE causes enhanced collisions of electrons to the wall and decreases the Hall parameter, which in turn further reduces the electron azimuthal velocity.

Although it cannot be directly captured in a 1D simulation, a smaller electron azimuthal velocity can result in and be caused by a space charge limited sheath. When the sheath potential is lowered by strong SEE, the azimuthal component of electron drift can interact with the channel wall, which results in reduced azimuthal drift and enhanced electron collision frequency in the axial direction. As a result of the slow azimuthal drift, the plasma may not be uniform in the azimuthal direction.[7] A possible mechanism of the stable mode is as follows: The collision frequency increases due to the space charge limited sheath, the electron mobility increases due to the decreased Hall parameter near the channel exit, and hence the plasma is confined in the ionization region inside the channel.

On the other hand, the breathing mode indicates that the electron azimuthal velocity is larger than it is in the stable mode. A larger azimuthal drift can reduce the electron temperature and hence a space charge limited sheath is not formed. As the sheath potential is formed near the channel exit, the electrons can drift azimuthally without colliding with the wall. A breathing mode can be considered as an axial oscillation mode supported by a strong circulating azimuthal electron drift, which was observed by Tilinin.[31] A recent experimental observation of the increase in rotating spokes may also be caused by the increase in the electron azimuthal drift.[33]

The effective electron temperature that a Langmuir probe measurement can obtain is a collection of the electron current containing drift and the electron temperature. The measurements by Raitses *et al.* showed that the measured electron temperature can exceed the electron temperature that predicts a space charge limited sheath and goes up to 60 eV at maximum.[32] The present numerical results suggest that a strong azimuthal drift component can increase the electron mean energy (Eq. 13) more than the space charge limited sheath (for BN-SiO_2, $\sim$ 25 eV of effective electron temperature).

3. *Strong ionization mode*

In order to understand the stabilization mechanism of the axial discharge oscillation, it is worth investigating the other strong oscillation mode that is found at B $\geq$ 200 G in Fig. 5.

Figure 8 shows the plasma properties for B = 280 G exhibiting a strong ionization mode. This mode has been observed in various numerical simulations[18,20,22] and experimentally reported in the SPT-100.[5] Gascon *et al.*[5] showed that this mode occurs for a discharge voltage larger than 600 V for BN-SiO_2 and when different wall materials including alumina, silicon carbide, and graphite are used. The mechanism that triggers a strong ionization mode is different from a breathing mode.

Figure 8(a) shows a very fast consumption of the ground-state atoms and a slow resupply mechanism that is determined by the inflow speed. Metastables and ions rapidly increase due to the strong ionization and stay at low density over a relatively long time ($t \sim 50\mu s$). A strong ionization can be observed in the diffusion region near the anode as well as in the ionization region (see Figs. 8(b) and 8(c)). The strong ionization is also related to the large electron mean energy near the anode during the ionization burst in comparison to the other two modes as shown in Fig. 8(e). It is obvious that the plasma is not confined steadily inside the channel.

The most notable difference between the strong ionization mode and the other two modes is that the electron axial velocity is very small throughout the domain. It indicates that the electrons are not efficiently transported into the discharge channel. Since the electron axial velocity is small, the electron azimuthal drift decreases as well. As can be seen from Fig. 8(e) and using Eq. 13, the electron temperature inside the channel exceeds the temperature that forms a space charge sheath not only near the channel exit but also in the middle of the channel. This indicates that a strong SEE or a space charge limited sheath may be a

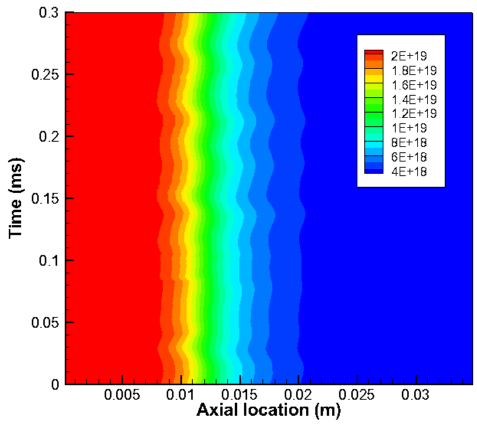

(a) Ground-state atom density (unit: m^{-3})

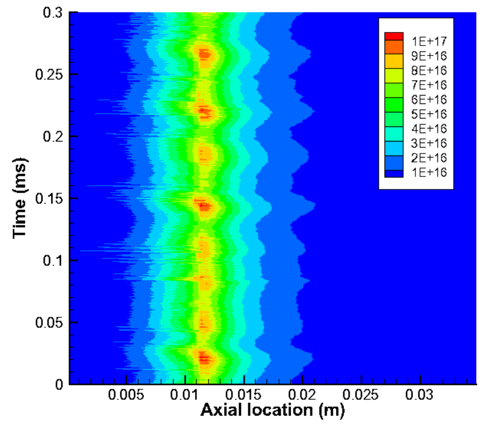

(b) Metastable density (unit: m^{-3})

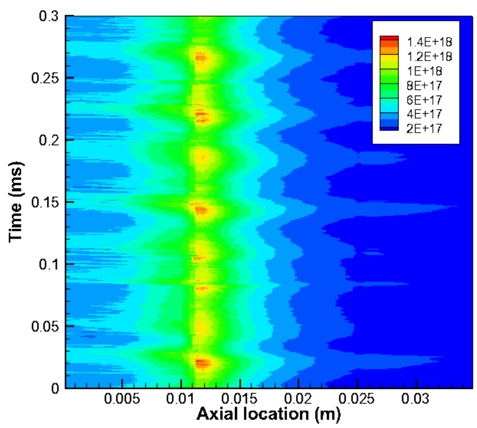

(c) Ion density (unit: m^{-3})

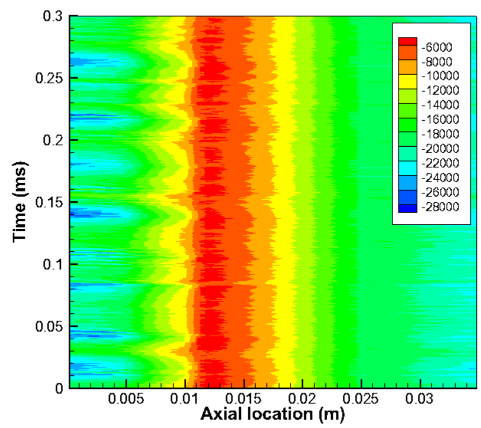

(d) Electron axial velocity (unit: m/s)

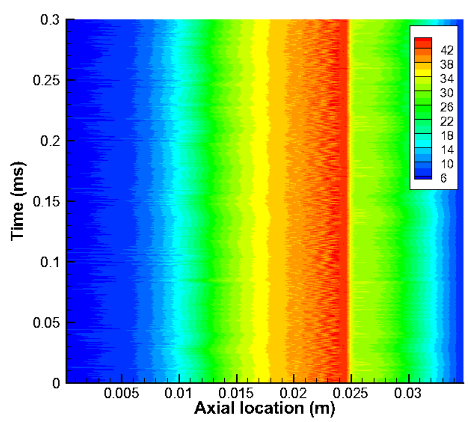

(e) Electron mean energy (unit: eV)

Figure 7. Stable mode: B = 180 G

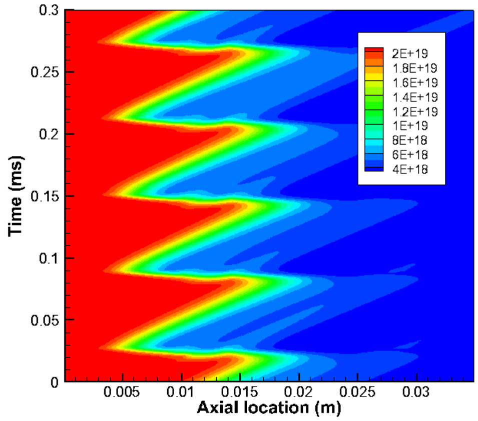

(a) Ground-state atom density (unit: m^{-3})

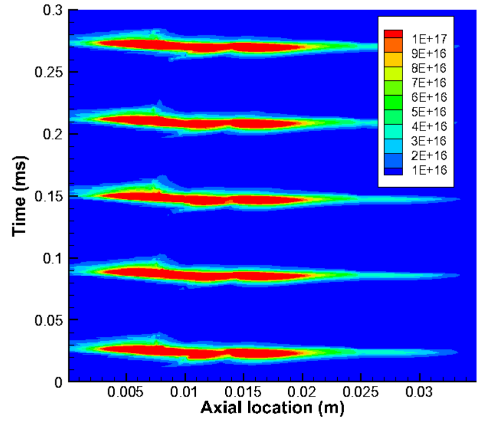

(b) Metastable density (unit: m^{-3})

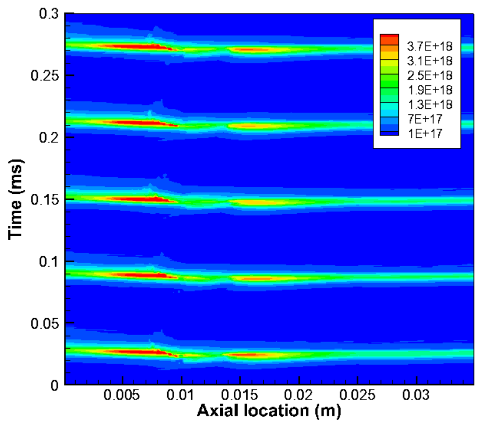

(c) Ion density (unit: m^{-3})

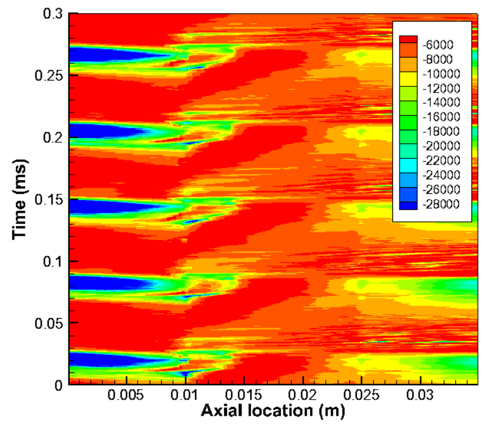

(d) Electron axial velocity (unit: m/s)

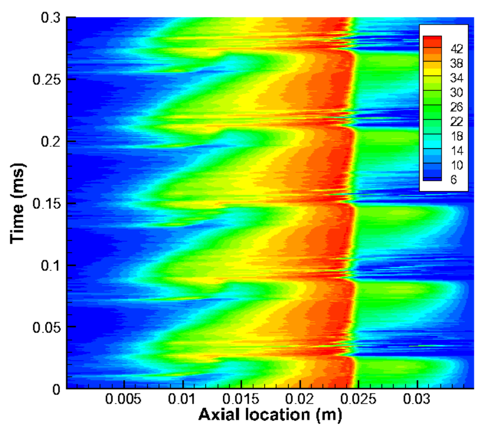

(e) Electron mean energy (unit: eV)

Figure 8. Strong ionization mode: B = 280 G

consequence of a stable mode but may not be the cause of stable operation. Even when the SEE effect is large, if the electrons are not supplied into the channel effectively, a strong ionization oscillation may occur.

The difference between this strong oscillation and the breathing mode is the supply mechanism of the electrons. A strong azimuthal drift is observed in a breathing mode and the stable mode is when the electron drift is optimized and stabilized whereas there is no strong electron azimuthal drift near the maximum of magnetic field in a strong ionization mode. The electron drift in the axial and azimuthal directions determines the confinement or stabilization of the plasma in the channel. Thus, the electron mobility that determines the electron drift plays a significant role in determining the electron flow axially and azimuthally. The sheath may be a result of stabilizing the plasma but a space charge limited sheath can also be present in a strong ionization mode.

C. Summary of mode transition

The breathing mode exhibits a strong electron drift both in the axial and azimuthal directions and the inability to confine the plasma due to the diffusion to the anode. In the stable mode, the plasma is well confined and steady in time although there remains a weak ionization oscillation that is more random and chaotic, which agrees with experimental observations. The electron temperature is large enough for a space charge limited sheath near the channel exit. The electron axial and azimuthal drifts are smaller than those in a breathing mode. It is indicated that the electron supply is optimized in the stable mode.

A strong ionization oscillation mode is caused by the insufficient electron supply into the channel due to the electron mobility. From our observations, this mode can be observed when the electron mobility near the anode is very small, when the electron mobility inside the channel is small and the magnetic field is large, or when the anomalous diffusion is weak in the near-plume. The balance between the electron mobility in all three regions determines the global discharge oscillations. It is also observed that this strong oscillation occurs even when a space charge limited sheath is formed. Thus, a space charge limited sheath per se may not be the cause of the mode transition from a breathing mode to a stable mode but may be a consequence of a steady mode. The electron mobility that determines the electron transport plays an important role in Hall thrusters. A self-consistent model that determines the electron mobility from the plasma parameters including magnetic field, plasma density, and electron temperature is required to understand the plasma oscillations in detail.

D. Light intensity

The light intensity is proportional to the metastable atom density:

$$Xe^* \rightarrow Xe + h\nu$$

Figure 9 shows the evolution of integrated number density of metastable atoms in the channel and the discharge current oscillation. The light intensity is strongly correlated with the discharge current, which agrees with the observation by Sekerak *et al.* in which a strong linear correlation between global light intensity and total discharge current is found (c.f. Figure 16 of Ref. 7). As shown in the previous section, the metastable density also strongly correlates with the ion density. Thus, the emitted light is linearly proportional to the plasma density. This may be of great interest to the experimentalists since measurement of visible light can be used to analyze the plasma oscillation without direct measurement.

In addition, it can be seen that the total light intensity, which can be obtained by integrating the metastable atom density over time, is larger in the stable mode than in the breathing mode although the peak intensity in the breathing mode is twice larger. The mean metastable atom density is 1.73×10^{16} m^{-3} for a breathing mode and 1.81×10^{16} m^{-3} for a stable mode. This indicates that the stable mode generates excited state (and ions) more efficiently.

Figure 10 depicts the correlation between the light intensity and discharge current. The light intensity is directly obtained from the normalized metastable atom density ($n^*/1 \times 10^{16}$ m^{-3}), where n^* is the metastable atom density. The strong correlation of the light and discharge current is again shown in the figure. However, it can be seen that the correlation coefficient is different in each mode. In the breathing mode, a strong light emission corresponds to a large discharge current.

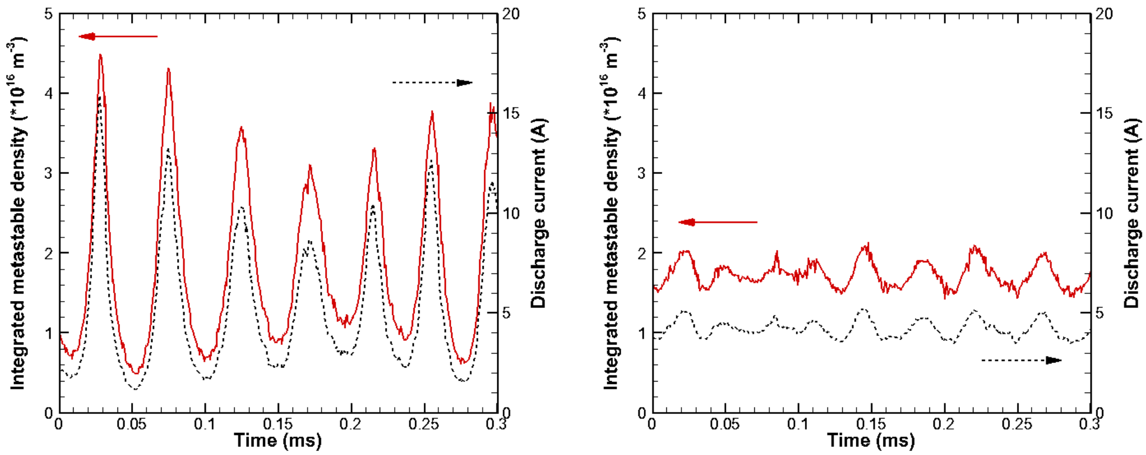

(a) Breathing mode: B = 120 G

(b) Stable mode: B = 180 G

Figure 9. Metastable density and discharge current: Red solid lines are the integrated metastable atom density; black dashed lines are discharge current. Two figures are on same scale.

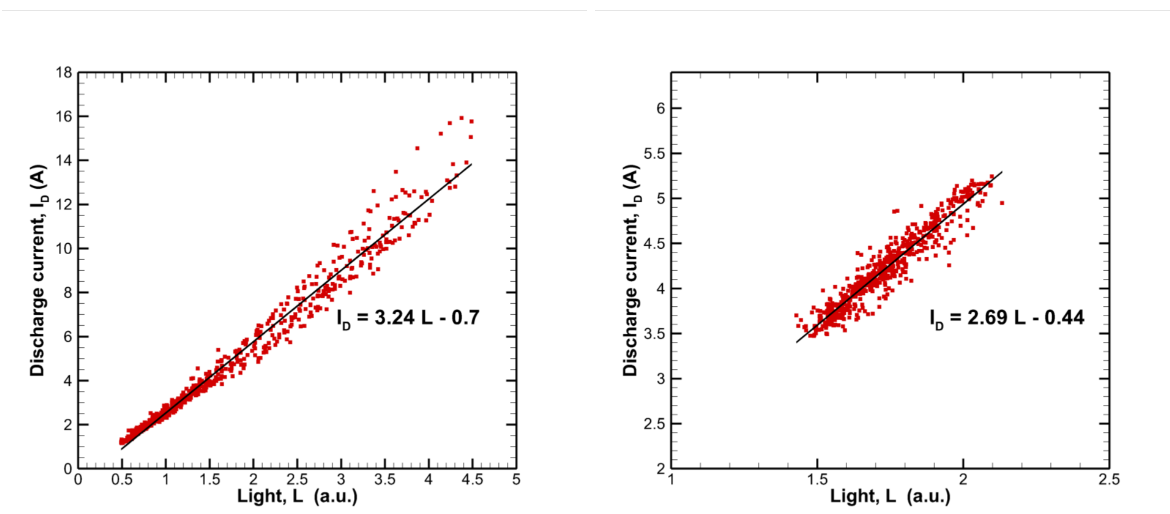

(a) Breathing mode: B = 120 G

(b) Stable mode: B = 180 G

Figure 10. Correlation between light intensity and discharge current: The light intensity $L = n^*/10^{16}$

E. Spontaneous emission rate

The effect of the metastable modeling in a Hall thruster is discussed in this section. As shown in Sec. II-B, the emission rate of a metastable in the present model is chosen as 1×10^7 s^{-1} based on taking a rate coefficient from the other processes. The sensitivity of the emission rate from a metastable to the ground state is investigated.

Figure 11 shows the discharge current oscillation when varying the spontaneous emission rate coefficient from 1×10^6 s^{-1} to 2×10^7 s^{-1} while keeping other numerical parameters the same values. As the emission rate is lowered, a strong ionization oscillation mode is observed. For 5×10^6 s^{-1}, the oscillation mode is a breathing mode. For the last two cases, the breathing mode oscillations are nearly damped out and a stable mode can be observed.

A conclusion that can be made from this section is that the metastable population also plays an important role in determining the plasma properties and plasma transport in a Hall thruster. It is suggested that all numerical frameworks should at least include one type of excited species in a Hall thruster simulation. However, in this paper one metastable atom is only taken into consideration. There are more excited levels in the xenon energy diagram as shown in Ref. 12. As future work, it is suggested that the other excited states should be included.

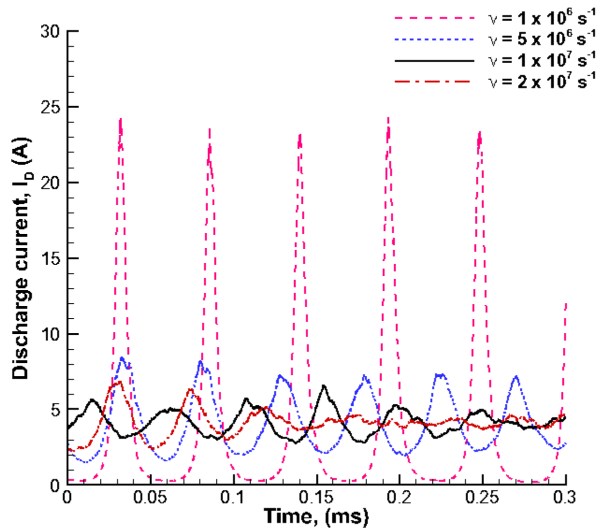

Figure 11. Discharge oscillation mode with different de-excitation collision frequencies for B = 185 G (stable mode).

F. Anomalous diffusion

The effect of the anomalous diffusion is investigated in this section. It is assumed in this study that the effect due to anomalous diffusion inside the channel is smaller than in the plume based on the experimental observations on the P5 thruster[21] and the H6 thruster.[19] It is considered that momentum loss due to the plasma-wall interaction dominates inside the channel, in particular in the acceleration region near the channel exit. Although the present model is not a self-consistent model that determines the electron mobility due to turbulence or high frequency oscillations, the trend of the discharge oscillations can be discussed by varying the anomalous mobility parameters.

In Sec. IV-A, the numerical results did not agree with the experimental observed behavior in low magnetic fields (B $\leq$ 110 G) and high magnetic fields (B $\geq$ 200 G). The attempt in this section is to vary the anomalous diffusion coefficient and examine the possible transition of anomalous diffusion coefficient depending on the magnetic field. Table 2 shows the three different cases considered. Case 1 uses low anomalous mobility outside the channel, which is expected at low magnetic fields. Case 2 is the nominal condition. Case 3 employs high anomalous mobility inside the channel, which is likely to occur at high magnetic fields.

Table 2. Anomalous mobility coefficient

ν_{ano}	Case 1	Case 2	Case 3
Inside	$\frac{1}{160}\omega_B$	$\frac{1}{160}\omega_B$	$\frac{1}{64}\omega_B$
Outside	$\frac{1}{40}\omega_B$	$\frac{1}{16}\omega_B$	$\frac{1}{16}\omega_B$

Figure 12 shows the comparison of the discharge current for all cases. As shown in Sec. IV-A, the nominal case (Case 2) shows mode transition from a steady mode to a breathing mode near B = 135 G, which is also found in experiments. However, another mode transition from a breathing mode to a stable mode is found at much lower magnetic field (B $\leq$ 110 G). Tilinin indicated that the classical mobility dominates over anomalous mobility at low magnetic fields.[31] Thus, a strong anomalous mobility may not represent the plasma behavior in such regimes. A breathing mode is found at B $\leq$ 120 G in Case 1 when the anomalous mobility outside the channel exit is reduced by a factor of 2.5 relative to Case 2. A reduced anomalous diffusion at low magnetic fields is a reasonable assumption given that the classical conductivity becomes dominant.

For a high magnetic field (B $\geq$ 200 G), a strong ionization oscillation is observed in Case 2. Even in Case 1, a strong ionization mode is found in such magnetic fields. As shown in Fig. 8, these strong oscillations occur due to the small electron axial velocity. The smaller the electron axial velocity, the more contribution from the sink term of the energy equation (Eq. 12), and the peak electron temperature moves inside the channel. Strong ionization is shown in the diffusion region near the anode (see Figs. 8(a), 8(b), and 8(c)). The plasma is not confined inside the channel. A possible explanation of this transition from a stable mode to a strong ionization mode is that the electron mobility model cannot account for the chaotic motion of plasma at high magnetic fields when a set of fixed values is used, which is also typically done in the-state-of-art Hall thruster simulations. For instance, a relatively high frequency oscillation observed at B = 180 G that may form a space charge limited sheath is likely to enhance the electron conductivity of the plasma near the channel exit.[34] A stable mode is observed at high magnetic fields (B $\geq$ 200 G) in Case 3 where the anomalous mobility coefficient is larger than Case 2.

Anomalous mobility plays an important role in Hall thruster operation. In order to capture regions I and V described in Section IV-A, it is suggested that the anomalous mobility coefficient outside the channel decreases as the Hall thruster transits from region II (transit regime) to region I (electron drift regime) as shown in Case 1. The anomalous mobility inside the channel increases at higher magnetic fields (B $\geq$ 200 G) where the mode transition occurs from regime III (optimal regime) to regime V (magnetic saturation regime) as shown in Case 3. It is required to have an anomalous mobility model not based on empirical values but as a function of the plasma parameters such as the magnetic field, plasma density, background density, electron temperature, and high frequency fluctuations.

The numerical frameworks developed so far assume fixed anomalous diffusion/mobility coefficients in each region but Fig. 12 suggests that the anomalous mobility coefficients should vary depending on the plasma parameters. Some anomalous diffusion theories justify our choice of the anomalous diffusion coefficient. Taylor and McNamara[35] showed from a two-dimensional turbulence theory that the anomalous diffusion is dependent on the plasma parameters.

$$D_{ano} = \frac{<(\Delta x)^2>}{\Delta t} = \frac{k_B T}{eB}\left(\frac{1}{2\pi n \lambda^2}\ln\frac{L}{2\pi\lambda}\right)^{1/2}$$

where n is the plasma density, λ is the Debye length, and L is the size of the plasma. Thus, the anomalous mobility coefficient is proportional to $T_e^{-1/2}$. It can be seen from this equation that the large electron temperature inside the channel makes the diffusion coefficient in that region smaller than that in the near-plume where the electron temperature is smaller. Yoshikawa and Rose[23] showed that the anomalous diffusion coefficient can be written as

$$D_{ano} = \frac{\pi}{4}\frac{<(n-n_0)^2>}{n_0^2}\frac{k_B T}{B}$$

in terms of the fluctuation of the plasma. The larger the fluctuation is, the larger the anomalous diffusion becomes. It has been also suggested from these relations that anomalous diffusion increases when the neutral atom density is small (or the background pressure is small) and the magnetic field is strong.

V. Conclusions

A hybrid-direct kinetic (DK) simulation has been developed to model the discharge plasma of an SPT-100 Hall thruster. It has been shown that the DK solver achieves reduced statistical noise relative to particle simulations. A new front tracking scheme has been developed in order to reduce the numerical error that propagates in the calculation domain. In addition, transport of the electronically excited atoms is taken into account in the present model.

The discharge current oscillation is investigated using a fixed anomalous diffusion model for a discharge voltage of 300 V and mass flow rate of 5 mg/s. Using anomalous mobility coefficients of 1/160 and 1/16

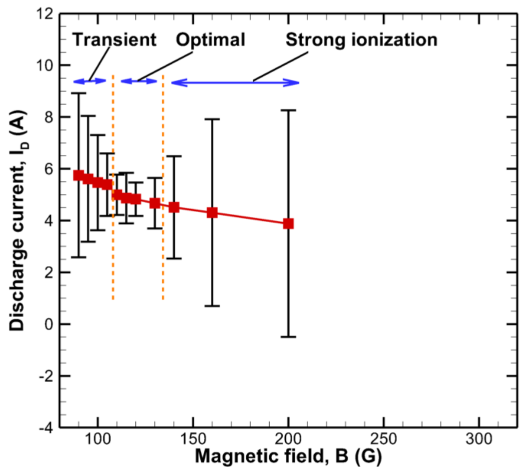

(a) Case 1 (low anomalous mobility)

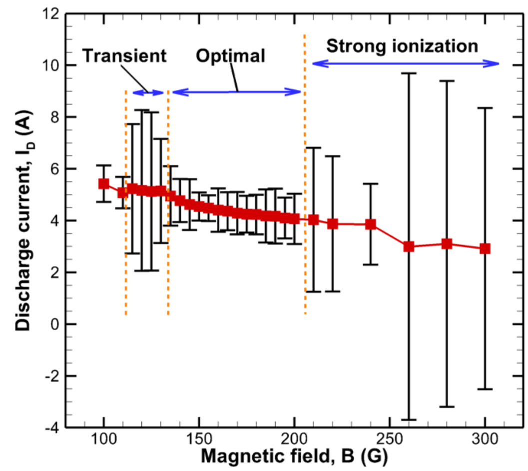

(b) Case 2 (nominal)

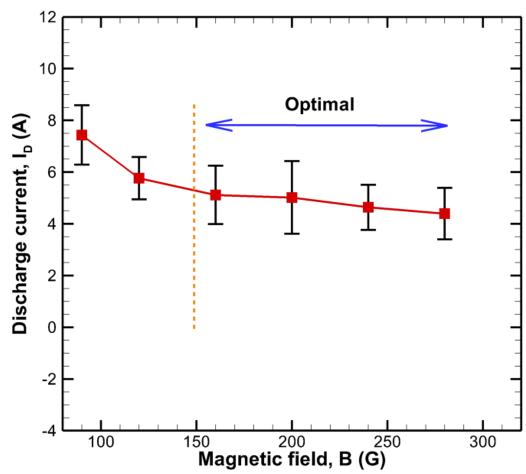

(c) Case 3(high anomalous mobility)

Figure 12. Varying anomalous diffusion coefficients.

inside and outside the channel, respectively, the transition from a breathing mode and stable mode at optimal magnetic fields (110 G $\leq$ B $\leq$ 200G) is observed. A moderate ionization oscillation is observed in the breathing mode. The possible mechanism for the transition from a stable mode to a breathing mode is that the plasma is electron starving, which can be seen from the large electron axial current in the near-plume and inside the channel.

In the stable mode, all the plasma properties are stable in time but some fluctuations are still present. The plasma is confined in the channel due to the balance of electron mobility near the anode, inside the channel, and in the near-plume. The numerical results also support the suggestion by Barral *et al.* that a space charge limited sheath may be associated with the mode transition. However, since a space charge limited sheath is also observed in a strong ionization mode, the space charge limited sheath may not be a sufficient condition for stabilizing the plasma oscillation but may be a necessary condition for a stable mode. There are two possible mechanisms that confine the plasma in a Hall thruster. One is that the enhanced collision frequency induced by strong SEE only near the channel exit increases the electron mobility in the acceleration region and the plasma confinement is effectively achieved in the ionization region. The other is the reduced electron azimuthal drift, also correlated with the electron drift in the axial direction and the Hall parameter. A large azimuthal drift may be associated with a breathing mode. The increase in electron mass flow, such as increase in cathode mass flow rate, may result in a reduced electron azimuthal velocity and stablize the oscillation, which has been observed experimentally by Brown and Gallimore.[8]

Modeling of the metastables could be very useful to validate light intensity measurements. A strong correlation between the discharge current and the metastable density, which is linearly proportional to the light intensity due to spontaneous emission, is found in a breathing mode and a stable mode, which agrees with recent experimental measurements. In addition, it is shown that the effect of metastable modeling on the discharge plasma behavior is significant. When the spontaneous emission rate of metastable atoms is varied, different oscillation modes are observed. The interactions with the other excited states may also play a significant role in determining the plasma oscillations.

The possibility of change in anomalous diffusion coefficients depending on the magnetic field strength is discussed. At a very small magnetic field (B $\leq$ 110 G), the classical conductivity dominates over anomalous diffusion. Thus, it is natural to consider that the contribution from anomalous diffusion decreases. On the other hand, at a large magnetic field (B $\geq$ 200 G), the anomalous diffusion inside the channel can be stronger due to the electron temperature saturation and instabilities that may occur from a space charge limited sheath. In order to understand the plasma physics in a Hall thruster, the anomalous diffusion coefficient should be considered not as a fixed parameter but as a function of the plasma parameters including magnetic field, plasma density, and electron temperature.

Acknowledgments

The authors gratefully acknowledge the financial support for this work provided by the U.S. Department of Energy Office of Science, Fusion Energy Sciences Program, Grant DESC0001939, and the Air Force Research Laboratory Grant F9550-09-1-0695. The first author thanks S. Barral for generously sharing his 1D fluid code and M. Sekerak for his insights and comments.

References

[1]Choueiri, E. Y., "Plasma Oscillations in Hall Thrusters," *Physics of Plasmas*, Vol. 8, 2001, pp. 1411–1426.

[2]Hara, K., Boyd, I. D., and Kolobov, V. I., "One-dimensional hybrid-direct kinetic simulation of the discharge plasma in a Hall thruster," *Physics of Plasmas*, Vol. 19, July 2012, pp. 113508.

[3]Kolobov, V. I. and Arslanbekov, R. R., "Towards Adaptive Kinetic-Fluid Simulations of Weakly Ionized Plasmas," *Journal of Computational Physics*, Vol. 231, No. 3, 2011, pp. 839–869.

[4]Berger, R. L., Brunner, S., Chapman, T., Divol, L., Still, C. H., and Valeo, E. J., "Electron and ion kinetic effects on non-linearly driven electron plasma and ion acoustic waves," *Physics of Plasmas*, Vol. 20, No. 3, 2013, pp. 032107.

[5]Gascon, N., Dudeck, M., and Barral, S., "Wall material effects in stationary plasma thrusters. I. Parametric studies of an SPT-100," *Physics of Plasmas*, Vol. 10, No. 10, 2003, pp. 4123–4136.

[6]Barral, S., Makowski, K., Peradzynski, Z., Gascon, N., and Dudeck, M., "Wall material effects in stationary plasma thruster. II. Near-wall and in-wall conductivity," *Physics of Plasmas*, Vol. 10, No. 10, October 2003, pp. 4137–4152.

[7]Sekerak, M. J., Longmier, B. W., Gallimore, A. D., Brown, D. L., Hofer, R. R., and Polk, J. E., "Mode Transitions in Hall Effect Thrusters," AIAA 2013-4116, San Jose, CA, July 2013.

[8]Brown, D. L. and Gallimore, A., "Investigation of Low Discharge Voltage Hall Thruster Operating Modes and Ionization Processes," IEPC-2009-074, Ann Arbor, MI, September 2009.

[9]Mitrofanova, O. A., Gnizdor, R. Y., Murashko, V. M., Koryakin, A. I., and Nesterenko, A. N., "New Generation of SPT-100," IEPC 2011-041, Wiesbaden, Germany, September 2011.

[10]McDonald, M., Bellant, C., Pierre, B. S., and Gallimore, A., "Measurement of Cross-Field Electron Current in a Hall Thruster Due to Rotating Spoke Instabilities," AIAA 2011-5810, San Diego, CA, August 2011.

[11]Raitses, Y., Griswold, M., Ellison, L., Parker, J., and Fisch, N. J., "Studies of Rotating Spoke Oscillations in Cylindrical Hall Thrusters," AIAA 2012-4179, Atlanta, GA, July 2012.

[12]Meunier, J., Belenguer, P., and Boeuf, J. P., "Numerical model of an ac plasma display panel cell in neon-xenon mixtures," *Journal of Applied Physics*, Vol. 78, No. 2, 1995, pp. 731–745.

[13]Puech, V. and Mizzi, S., "Collision Cross Sections and Transport Parameters in Neon and Xenon," *J. Phys. D: Appl. Phys.*, Vol. 24, 1991, pp. 1974–1985.

[14]Rapp, D. and Englander-Golden, P., "Total Cross Sections for Ionization and Attachment in Gases by Electron Impact. I. Positive Ionization," *The Journal of Chemical Physics*, Vol. 43, No. 5, 1965, pp. 1464–1479.

[15]Ton-That, D. and Flannery, M. R., "Cross sections for ionization of metastable rare-gas atoms (Ne*, Ar*, Kr*, Xe*) and of metastable N_2*, CO* molecules by electron impact," *Phys. Rev. A*, Vol. 15, Feb 1977, pp. 517–526.

[16]Ahedo, E., Martinez-Cerezo, P., and Martinez-Sanchez, M., "One-dimensional model of the plasma flow in a Hall Thruster," *Physics of Plasmas*, Vol. 8, No. 6, June 2001, pp. 3058–3068.

[17]Hayashi, M., "Determination of electron-xenon total excitation cross-sections, from threshold to 100 eV, from experimental values of Townsend's ," *Journal of Physics D: Applied Physics*, Vol. 16, No. 4, 1983, pp. 581.

[18]Barral, S. and Ahedo, E., "Low-frequency model of breathing oscillations in Hall discharges," *Phys. Rev. E*, Vol. 79, Apr 2009, pp. 046401.

[19]Hofer, R. R., Katz, I., Mikellides, I. G., Goebel, D. M., Jameson, K. K., Sullivan, R. M., and Johnson, L. K., "Efficacy of Electron Mobility Models in Hybrid-PIC Hall Thruster Simulations," AIAA 2008-4924, Hartford, CT, July 2008.

[20]Bareilles, J., Hagelaar, G. J. M., Garrigues, L., Boniface, C., Boeuf, J. P., and Gascon, N., "Critical assessment of a two-dimensional hybrid Hall thruster model: Comparisons with experiments," *Physics of Plasmas*, Vol. 11, No. 6, June 2004, pp. 3035–3046.

[21]Koo, J. W. and Boyd, I. D., "Modeling of anomalous electron mobility in Hall thrusters," *Physics of Plasmas*, Vol. 13, No. 033501, 2006.

[22]Hagelaar, G. J. M., Bareilles, J., Garrigues, L., and Boeuf, J. P., "Two-dimensional model of a stationary plasma thruster," *Journal of Applied Physics*, Vol. 91, No. 9, May 2002, pp. 5592–5598.

[23]Yoshikawa, S. and Rose, D. J., "Anamalous Diffusion of a Plasma across a Magnetic Field," *Physics of Fluids*, Vol. 5, No. 3, March 1962, pp. 334–40.

[24]Goebel, D. and Katz, I., *Fundamentals of Electric Propulsion: Ion and Hall Thrusters*, Wiley, 2008.

[25]Cheng, C. and Knorr, G., "The integration of the vlasov equation in configuration space," *Journal of Computational Physics*, Vol. 22, No. 3, 1976, pp. 330 – 351.

[26]Arora, M. and Roe, P. L., "A Well-Behaved {TVD} Limiter for High-Resolution Calculations of Unsteady Flow," *Journal of Computational Physics*, Vol. 132, No. 1, 1997, pp. 3 – 11.

[27]Boeuf, J. P. and Garrigues, L., "Low Frequency Oscillations in a Stationary Plasma Thruster," *Journal of Applied Physics*, Vol. 84, No. 7, 1998, pp. 3541–3554.

[28]Garrigues, L., Boyd, I. D., and Boeuf, J. P., "Computation of Hall Thruster Performance," *Journal of Propulsion and Power*, Vol. 17, No. 4, July 2001, pp. 772–779.

[29]Gascon, N., Perot, C., Bonhomme, G., Caron, X., Bechu, S., Lasgorceix, P., Izrar, B., and Dudeck, M., "Signal processing and non-linear behavior of a stationary plasma thruster: First results," AIAA 1999-2427, Los Angeles, CA, June 1999.

[30]Bechu, S., Perot, C., Gascon, N., Lasgorceix, P., Hauser, A., and Dudeck, M., "Operating mode investigation of a Laboratory Stationary Plasma Thruster," AIAA 1999-2567, Los Angeles, CA, June 1999.

[31]Tilinin, G. N., "High-frequency plasma waves in a Hall accelerator with an extended acceleration zone," *Sov. Phys. Tech. Phys.*, Vol. 22, 1977, pp. 974–978.

[32]Raitses, Y., Staack, D., Smirnov, A., and Fisch, N. J., "Space charge saturated sheath regime and electron temperature saturation in Hall thrusters," *Physics of Plasmas*, Vol. 12, No. 7, 2005, pp. 073507.

[33]Sekerak, M. J., Longmier, B. W., Gallimore, A. D., Brown, D. L., Hofer, R. R., and Polk, J. E., "Azimuthal Spoke Propagation in Hall Effect Thrusters," IEPC 2013-143, Washinton D.C., September 2013.

[34]Campanell, M. D., Khrabrov, A. V., and Kaganovich, I. D., "General Cause of Sheath Instability Identified for Low Collisionality Plasmas in Devices with Secondary Electron Emission," *Phys. Rev. Lett.*, Vol. 108, Jun 2012, pp. 235001.

[35]Taylor, J. B. and McNamara, B., "Plasma Diffusion in Two Dimensions," *Physics of Fluids*, Vol. 14, No. 7, 1971, pp. 1492–1499.